

# Nerve Guidance Conduits Based on Double-Layered Scaffolds of Electrospun Nanofibers for Repairing the Peripheral Nervous System

Jingwei Xie,<sup>†,‡,§</sup> Matthew R. MacEwan,<sup>†,‡</sup> Wenyi Liu,<sup>‡</sup> Nithya Jesuraj,<sup>†</sup> Xiaoran Li,<sup>†</sup> Daniel Hunter,<sup>§</sup> and Younan Xia<sup>\*,||,‡</sup>

<sup>†</sup>Department of Biomedical Engineering, Washington University, St. Louis, Missouri 63130, United States

<sup>‡</sup>School of Chemical and Biomolecular Engineering, Georgia Institute of Technology, Atlanta, Georgia 30332, United States

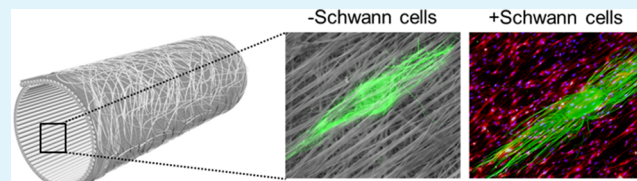
<sup>§</sup>Division of Plastic and Reconstructive Surgery, Department of Surgery, Washington University School of Medicine, St. Louis, Missouri 63110, United States

<sup>||</sup>The Wallace H. Coulter Department of Biomedical Engineering, Georgia Institute of Technology and Emory University; School of Chemistry and Biochemistry, Georgia Institute of Technology, Atlanta, Georgia 30332, United States

## Supporting Information

**ABSTRACT:** Compared to the nerve guidance conduits (NGCs) constructed from a single layer of aligned nanofibers, bilayer NGCs with random and aligned nanofibers in the outer and inner layers are more robust and tear-resistant during surgical procedures thanks to an isotropic mechanical property provided by the random nanofibers. However, it remains unclear whether the random nanofibers will interfere with the aligned nanofibers to alter the extension pattern of the neurites and impede regeneration. To answer this question, we seeded dorsal root ganglia (DRG) on a double-layered scaffold, with aligned and random nanofibers on the top and bottom layers, respectively, and evaluated the outgrowth of neurites. The random nanofibers in the bottom layer exerted a negative impact on the extension of neurites projecting from the DRG, giving neurites a less ordered structure compared to those cultured on a single layer of aligned nanofibers. The negative impact of the random nanofibers could be effectively mitigated by preseeding the double-layered scaffold with Schwann cells. DRG cultured on top of such a scaffold exhibited a neurite outgrowth pattern similar to that for DRG cultured on a single layer of aligned nanofibers. We further fabricated bilayer NGCs from the double-layered scaffolds and tested their ability to facilitate nerve regeneration in a rat sciatic nerve injury model. Both histomorphometric analysis and functional characterization demonstrated that bilayer NGCs with an inner surface that was preseeded with Schwann cells could reach 54%, 64.2%, and 74.9% of the performance of isografts in terms of nerve fiber number, maximum isometric tetanic force, and mass of the extensor digitorum longus muscle, respectively. It can be concluded that the bilayer NGCs hold great potential in facilitating motor axon regeneration and functional motor recovery.

**KEYWORDS:** *electrospun nanofiber, neurite extension, nerve guidance conduit, peripheral nerve repair, regenerative medicine, neural tissue engineering*



## INTRODUCTION

Severe injuries to the peripheral nervous system (PNS) often result in a lesion in the nerves.<sup>1,2</sup> For lesions longer than 4 mm, end-to-end anastomosis is no longer an option because it generates detrimental tension along the nerves and retards healing.<sup>3</sup> In these cases, interposing a graft between the proximal and distal stumps is expected to provide better regenerative outcomes.<sup>4</sup> Autografts are the current gold standard for peripheral nerve repair, as they provide abundant supporting cells for the regrowth of regenerated axons and offer intact intraluminal guidance along the longitudinal direction. However, the use of an autograft is plagued by a number of clinical limitations, including the morbidity of the donor site, the limited availability of graft material, the mismatch in size, and the necessity for multiple surgeries.<sup>5–7</sup> Development of alternative treatments is therefore highly desirable. Synthetic nerve guidance conduits (NGCs), with the intraluminal

presence of longitudinal contact guidance and supporting glial cells, can mimic the structure and composition of an autograft and can even potentially match the performance of an autograft in terms of regeneration.<sup>8–10</sup> NGCs with such features have been investigated by a number of research groups,<sup>11–13</sup> with NGCs composed of electrospun nanofibers being the most promising candidates.

Electrospun nanofibers represent a new class of synthetic nanomaterials with the capability to mimic the hierarchical structure of the extracellular matrix (ECM). Most importantly, electrospun nanofibers can be readily collected as uniaxially aligned arrays,<sup>14–18</sup> providing topographical cues to direct and enhance axonal extension during regeneration. Furthermore, by

Received: March 27, 2014

Accepted: May 7, 2014

Published: May 7, 2014

controlling their size, alignment, and stacking, scaffolds made of electrospun nanofibers can be easily adapted for direct implantation.<sup>19</sup> These unique features make electrospun nanofibers an intriguing class of scaffolds with unique applications in neural tissue engineering. In most studies, uniaxially aligned nanofibers were collected as a rectangular sheet, rolled up, and sealed at the overlapping edges to obtain an NGC, with the direction of fiber alignment parallel to the longitudinal direction of the conduit.<sup>9,11</sup> Although this type of NGC can provide good guidance along the longitudinal axis, its surgical handling has been a challenge. During coadaptation, a suture needs to travel through the wall of an NGC multiple times when securing a nerve stump into the NGC. Frequent piercing makes the wall of the NGC prone to tearing along the direction of fiber alignment, especially when force is applied to bring the nerve stump into the NGC. As a result, it is necessary to develop nanofiber-based NGCs with more tear-resistant walls to meet the requirements of current surgical procedures. Such an NGC will not only provide longitudinal contact guidance for axonal extension but also deliver a wall robust enough to withstand the surgical operation.

To this end, our group recently developed a new type of NGC by rolling two layers of electrospun nanofibers into a tube, with the top and bottom layers containing uniaxially aligned and random fibers, respectively. The random nanofibers provide an isotropic mechanical property for the NGC and render the conduit tear-resistant during a surgical procedure, whereas the aligned nanofibers serve the role of guiding the axons during regrowth. While the surgical feasibility of this new type of NGC has been demonstrated by our group,<sup>11</sup> the possible negative impact of the random nanofibers on the extension of axons remains to be resolved. For instance, whether the random fibers will interfere with the aligned fibers to alter the outgrowth pattern of the neurites is yet to be investigated. Moreover, in an effort to recapitulate the composition of an autograft, the bilayer NGCs should be seeded with supporting glial cells prior to implantation. It remains unclear if these supporting cells will influence the guided outgrowth of neurites. A full assessment of these issues is critical to the successful implementation of bilayer NGCs in peripheral nerve repair.

In the present work, we used dorsal root ganglia (DRG) as a model system to investigate the patterns of neurite outgrowth on (i) a pristine double-layered scaffold, with uniaxially aligned and random fibers in the top and bottom layers, respectively, and (ii) a double-layered scaffold preseeded with primary Schwann cells, a type of glial cell in the PNS. Using a sciatic nerve transaction/repair model, we further examined the regenerative potential of bilayer NGCs constructed from the double-layered scaffolds *in vivo*. This work represents a logical step toward the development of synthetic bilayer NGCs that are not only reliable during surgical procedures but also promising in terms of nerve regeneration and functional recovery.

## MATERIALS AND METHODS

**Fabrication of Nanofiber-Based Scaffolds by Electrospinning.** Nanofibers were produced using an electrospinning setup similar to what was reported previously.<sup>20–22</sup> Briefly, a 20% (w/v) solution of poly(*ε*-caprolactone) (PCL) was prepared by dissolving the polymer in a 4:1 mixture of dichloromethane (DCM) and *N,N*-dimethylformamide (DMF) (Fisher, Pittsburgh, PA). The PCL solution was loaded into a syringe and pumped at a constant rate through a 22 gauge needle, while a 15 kV potential was applied

between the needle and a grounded collector. A glass coverslip and a U-shaped frame of stainless steel were employed to collect random and uniaxially aligned nanofibers, respectively. After electrospinning, the nonwoven mat of nanofibers was transferred onto a glass coverslip and fixed around the edges with Silastic Type A Medical Adhesive (Dow Corning, Midland, MI). Double-layered scaffolds were fabricated by placing a mat of aligned nanofibers on top of a mat of random nanofibers and then fixed around the edges. Prior to cell seeding, the scaffolds were placed in a 24-well tissue culture polystyrene (TCPS) plate and sterilized with 70% ethanol for 24 h.

**Schwann Cell Isolation, Expansion, and Seeding.** Mixed motor and sensory Schwann cells were isolated from the sciatic nerves harvested from 250 g male Lewis rats (Charles River, Wilmington, MA). The animals were anesthetized with 4% isoflurane/96% oxygen (induction) and 2% isoflurane/98% oxygen (maintenance). Following preparation and sterilization of the lateral aspects of both legs, the sciatic nerves were exposed bilaterally through dorsolateral gluteal muscle-splitting incisions, followed by blunt dissection. With an operating microscope, the sciatic nerves were then stripped of connective tissue, explanted, and placed directly in cold Leibovitz's L-15 medium (Sigma-Aldrich, St. Louis, MO). The explanted sciatic nerves were digested in a solution of 1% collagenase (Fisher) and 2.5% trypsin (Invitrogen, Carlsbad, CA) at 37 °C for 30 min. After centrifugation, the collected cells were washed and resuspended in the Dulbecco's modified Eagle medium (DMEM) supplemented with 10% heat-inactivated fetal bovine serum (FBS) and 1% antibiotic antimycotic (ABAM, Invitrogen). The resulting cells were plated on poly(L-lysine) (PLL) coated, 10 cm Petri dishes (Sigma-Aldrich). The Schwann cell cultures were purified by adding 10 μM cytosine-beta-arabino furanoside hydrochloride (Ara-C) into the medium (Sigma-Aldrich) on day 2 to kill the contaminating fibroblasts. On day 6, the cells were incubated with 40 μL (1:400 dilution in media) of rabbit antimouse polyclonal Thy 1.1 (Serotec, Raleigh, NC) at 37 °C for 20 min, followed by incubation with 400 μL (1:40 dilution in media) of guinea pig complement (Sigma-Aldrich) at 37 °C for 40 min.

Following adhesion to the culture plate, the Schwann cells were expanded by replacing the culture media with DMEM supplemented with FBS, ABAM, 2 μM forskolin (Sigma-Aldrich), and 20 g/mL of pituitary extract (PE) (Biomedical Tech Inc., Stoughton, MA) every 2 days. Upon reaching confluence, Schwann cell cultures were passaged by washing each culture flask twice with Hanks balanced salt solution (HBSS) (Invitrogen) prior to incubation with 0.25% trypsin-EDTA at 37 °C for 3 min. Following centrifugation at 134g for 5 min, the collected cells were resuspended, split 1:2, and replated on similar PLL-coated tissue culture dishes. Schwann cell cultures were expanded in this manner until an adequate number of cells were obtained.

Prior to seeding onto the scaffolds, the Schwann cells were resuspended in growth media containing DMEM supplemented with 10% FBS, 1% ABAM, 2 μM forskolin, and 20 mg/mL of PE to achieve a final concentration of  $5 \times 10^5$  cells/mL. The expanded Schwann cells were seeded by adding 1 mL of the cell suspension to each well of a 24-well culture plate and then incubated at 37 °C for 24 h to promote cell adhesion.

**Isolation and Culture of DRG.** It is critical to localize DRG specifically to the thoracic region of the spinal column in an effort to minimize the variation in cellular composition among the primary tissue cultures. In the present study, we consistently harvested all DRG from the thoracic region of the spinal column in embryonic white leghorn chicks via sterile microdissection. Specifically, the DRG were dissected from the thoracic spine of embryonic day 8 (E8, stage HH35-36). White leghorn chicks were collected in HBSS prior to plating. The isolated DRG were placed on the nanofiber scaffolds (1 DRG per scaffold) in the absence and presence of preseeded Schwann cells and subsequently cultured for 6 days in DMEM supplemented with 10% FBS, 1% ABAM, 2 μM forskolin, and 20 mg/mL of PE. Nanofiber scaffolds preseeded with Schwann cells but without DRG were similarly cultured for a period of 6 days as a control.

**Immunostaining and F-Actin Staining of Schwann Cells.** After culturing for 7 days, the Schwann cells were immunostained with anti-S100 antibody (Sigma-Aldrich) and Alexa Fluor 660 Phalloidin

(Invitrogen), respectively. The samples were fixed in 3.7% formaldehyde at room temperature for 45 min and permeabilized with 0.1% Triton X-100 for 30 min. For S-100 staining, the samples were blocked with PBS containing 5% normal goat serum (NGS) (Invitrogen) for 1 h, washed, and incubated with S-100 antibody diluted (1:200) in PBS containing 2% normal goat serum (NGS) (Invitrogen) overnight at 4 °C. The anti-S100 marker was detected using Cy5 goat anti-rabbit IgG (1:200; Invitrogen) secondary antibody. For F-actin staining, 5 μL of methanolic stock solution was diluted with 200 μL of PBS for each sample to be stained. To reduce nonspecific background staining with these conjugates, 1% bovine serum albumin (BSA) was added to the staining solution. Each sample was stained for 30 min at room temperature and washed twice with PBS. After staining, fluorescence images were taken using a QICAM Fast Cooled Mono 12-bit camera (Q Imaging) attached to an Olympus microscope with Capture 2.90 (Olympus, Center Valley, PA).

**Immunostaining of Dorsal Root Ganglia.** After culturing for 6 days, the DRG neurons were immunostained with anti- $\beta$ III tubulin antibody (Tuj1) (Covance, San Diego, CA). Briefly, the samples were fixed and blocked as described above and then incubated with antibody diluted (1:500) in PBS that contained 2% NGS overnight at 4 °C. The Tuj1 marker was detected using AlexaFluor 488 goat anti-mouse IgG (1:200; Invitrogen) secondary antibody and imaged as described above.

**Scanning Electron Microscopy.** Prior to cell seeding, the nanofiber scaffolds were sputter-coated with gold and imaged with a scanning electron microscope (Nova 200 NanoLab, FEI, Hillsboro, OR) at an accelerating voltage of 15 kV to confirm the morphology of individual PCL nanofibers within the scaffolds.

**Preparation of Nerve Guidance Conduits.** Double-layered scaffolds were fabricated by stacking aligned nanofibers on top of random nanofibers. A rectangular, double-layered scaffold was wrapped around a metal mandrel and sealed at the overlapping edges to obtain an NGC that was 2 mm in diameter and 16 mm in length. All NGCs were placed in 24-well TCPS plates and sterilized with 70% ethanol for 24 h. Following sterilization, all conduits were immersed in growth media containing DMEM supplemented with 10% FBS, 1% ABAM, 2 μM forskolin, and 20 mg/mL of PE. To be seeded with Schwann cells, the open ends of all NGCs were sealed with 10–0 nylon sutures and then loaded with 100 μL of a medium containing  $2 \times 10^6$  Schwann cells. The NGC was subsequently kept in culture for 6 days prior to in vivo implantation. The Schwann cell-loaded NGCs were axially rotated every 6–8 h for the first 3 days to ensure even distribution of Schwann cells across the luminal surface of the conduit.

**In Vivo Model of Nerve Transection and Repair.** Twenty four adult male Lewis rats were randomized into three groups (I–III) of six animals each ( $n = 6$ ). Group I served as the positive control in which sciatic nerve defects were repaired with 14 mm reversed nerve grafts obtained from an isogenic source, or isografts. Groups II and III served as experimental groups in which sciatic nerve defects were repaired with 16 mm NGCs and 16 mm Schwann cell-seeded NGCs, respectively. Groups II and III incorporated 1 mm of nerve on each end yielding critical 14 mm nerve gaps. Twelve weeks post-operatively all animals were anesthetized prior to undergoing functional assessment of motor recovery. All animals were subsequently euthanized, and sciatic nerves were harvested en bloc for histomorphometric evaluation.

**Surgical Procedures.** Rats were anesthetized via isoflurane gas (4% induction, 2% maintenance) prior to aseptic preparation and surgical exposure of the right sciatic nerve through a dorsolateral gluteal muscle-splitting incision. The sciatic nerve was transected 5 mm proximal to the trifurcation and then repaired with either 14 mm reversed isografts (Group I), 16 mm NGCs (Groups II), or 16 mm NGCs preseeded with Schwann cells (Group III). Nerve grafts were microsurgically sutured to the proximal and distal nerve stumps using one 10–0 nylon suture and secured with fibrin sealant (TISSEEL, Baxter International Inc., Deerfield, IL). NGCs were similarly interposed and secured to the proximal and distal nerve stumps using two 10–0 nylon sutures, such that 1 mm of the host nerve was

present at either end of the conduit. As a result, recipient nerves in all groups were challenged with a consistent 14 mm nerve gap. Following implantation, muscle fascia and skin were closed in two layers using 6–0 polyglactin and 4–0 nylon sutures, respectively.

Twelve weeks post-operation, all animals were anesthetized and prepared for in situ measurement of evoked muscle force. Operative sciatic nerves were reexposed as previously described. The distal portion of the right extensor digitorum longus (EDL) muscle was exposed through a skin incision extending from the dorsum of the foot to the knee. The distal tendons of the EDL muscle were subsequently transected and sutured to a metal S-hook using 5–0 nylon sutures. Both incisions were bathed in saline-soaked gauze to prevent desiccation during in situ functional assessment. Following testing, all animals were euthanized via intracardiac injection of sodium pentobarbital (>200 mg/kg, Somnafus). Operative sciatic nerves were then transected 4–5 mm proximal and 4–5 mm distal to interposed nerve grafts or conduits, explanted, and stored in 3% glutaraldehyde in 0.1 M phosphate buffer (pH 7.2) at 4 °C prior to histomorphometric analysis.

**Histological Assessment of Nerve Regeneration.** Harvested sciatic nerves were processed and analyzed as previously described.<sup>23</sup> Briefly, the nerves were post-fixed with 1% osmium tetroxide, serially dehydrated in ascending concentrations of ethanol, and embedded in Araldite S02 (Polyscience Inc., Warrington, PA). The blocked nerves were cut into 1 μm thick slices using an ultramicrotome and stained with 1% toluidine blue for light microscopy imaging and qualitative analysis. An observer blind to the present work measured total number of nerve fibers in cross-sections acquired 5 mm distal to the interposed nerve graft/conduit.

**Assessment of Functional Motor Recovery.** Sciatic nerve function was assessed by measuring the evoked motor response in reinnervated EDL muscle upon electrical stimulation of the repaired sciatic nerve. Animals were immobilized in an automated functional assessment station (FASt System, Red Rock Laboratories, St. Louis, MO) where the distal portion of the EDL muscle was fixed to a 5 N load cell. Cathodic, monophasic electrical impulses (duration = 200 μs, frequency = 0–200 Hz, burst width = 300 ms, amplitude = 0–1000 μA) were applied to the sciatic nerve proximal to the interposed nerve graft/conduit via microwire electrodes, while the resulting force production in the EDL was recorded using custom data acquisition software (RRL V.1.3, Red Rock Laboratories).

Elicited twitch contractions were utilized to determine the optimal stimulus amplitude ( $V_o$ ) and optimal muscle length ( $L_o$ ) for isometric force production in the EDL muscle. All subsequent isometric force measurements were made at  $V_o$  and  $L_o$ . Single twitch contractions were recorded, and maximum twitch force ( $F_t$ ) was calculated. Tetanic contractions were recorded at increasing frequencies of stimulation (5–200 Hz), allowing an interval of 2 min between stimuli to prevent muscle fatigue. Maximum isometric tetanic force ( $F_o$ ) was calculated from the resulting sets of recorded force traces. Following the assessments, both denervated/reinnervated and unoperative EDL muscles were harvested from each animal and weighed.

**Statistical Analysis.** Mean values and standard deviations are reported. Statistical analyses of neurite field eccentricity and maximum neurite length were performed using ANOVA, followed by a Scheffé's F post-hoc test at a 95% confidence level. Statistical comparisons between distributions of Schwann cell orientations were performed using a Kolmogorov–Smirnov test where  $p < 0.05$  was accepted as significant.

## RESULTS AND DISCUSSION

**Outgrowth of DRG Neurites on Single-Layered Scaffolds in the Absence and Presence of Preseeded Schwann Cells.** We first examined the extension of neurites from DRG cultured on single-layered scaffolds consisting of random PCL nanofibers (see the inset in Figure 1A for a typical SEM image) in the absence and presence of preseeded Schwann cells. Schwann cells were visualized by S-100 staining, which is a family of low-molecular-weight proteins found in

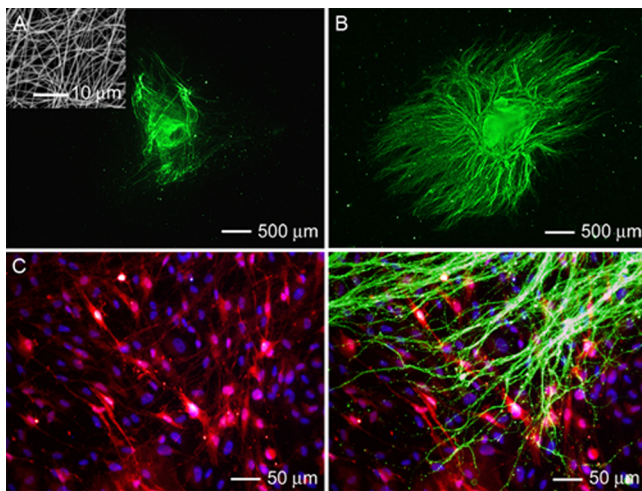


**Figure 1.** Fluorescence micrographs of typical neurite fields extending from DRG seeded on scaffolds made of random PCL nanofibers, in the (A) absence and (B) presence of preseeded Schwann cells. The neurites were stained with Tuj1 marker (green). Inset: SEM image of the random nanofibers. (C) Double staining of the Schwann cells in (B) with anti-S100 (red) and their nuclei with DAPI (blue). (D) Triple staining of the Schwann cells with anti-S100 (red), their nuclei with DAPI (blue), and the neurites with Tuj1 marker (green) for the sample shown in (B).

vertebrates and characterized by two calcium-binding sites. S-100 proteins have been implicated in a variety of intracellular and extracellular functions. S-100 proteins are involved in regulation of protein phosphorylation, transcription factors,  $\text{Ca}^{2+}$  homeostasis, the dynamics of cytoskeleton constituents, enzyme activities, cell growth and differentiation, and the inflammatory response.<sup>24</sup> S-100 is expressed in the cytoplasm of the Schwann cells and is a commonly used indicator of Schwann cell phenotypic characteristics.<sup>25,26</sup>

In both cases, neurites were observed to extend across the scaffolds with no preferred direction or orientation (Figure 1, A and B). In the absence of Schwann cells, only a few short neurites were projected from the cell body (Figure 1A). When the scaffold was preseeded with Schwann cells, more neurites were observed to grow from the cell body within the same culture time (Figure 1B). These neurites also showed a longer average length in comparison with those of DRG cultured in the absence of Schwann cells. For the DRG cultured in the absence and presence of preseeded Schwann cells, the neurites were  $378 \pm 13 \mu\text{m}$  and  $1232 \pm 325 \mu\text{m}$ , respectively, in average lengths (Figure S1, Supporting Information). The preseeded Schwann cells also exhibited a random pattern (Figure 1C). Triple staining of the Schwann cells, their nuclei, and the neurites indicate that the neurites were largely extended along the preseeded Schwann cells (Figure 1D).

The extension of neurites from DRG cultured on single-layered scaffolds made of uniaxially aligned PCL nanofibers (see the inset in Figure 2A for a typical SEM image) displayed a different pattern compared to DRG cultured on scaffolds consisting of random nanofibers (Figure 2). In both the absence and presence of preseeded Schwann cells, the neurites projecting from the cell body were guided to extend parallel to the nanofibers (Figure 2, A and B). As a result, the neurites displayed a high degree of eccentricity and directional specificity that was not observed for DRG cultured on random nanofibers. Preseeding of Schwann cells notably increased both

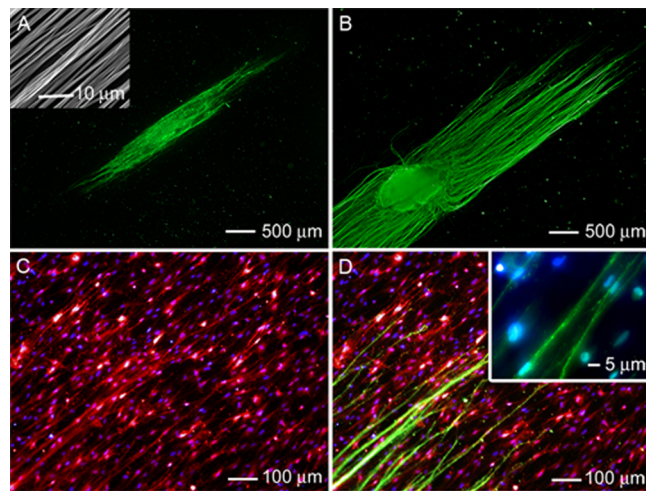


**Figure 2.** Fluorescence micrograph of a typical neurite field extending from DRG seeded on aligned PCL nanofiber scaffolds in the (A) absence and (B) presence of preseeded Schwann cells. The neurites were stained with Tuj1 marker (green). Inset: SEM image of the aligned nanofibers. (C) Double staining of the Schwann cells in (B) and their nuclei with anti-S100 (red) and DAPI (blue). (D) Triple staining of the Schwann cells with anti-S100 (red), their nuclei with DAPI (blue), and the neurites with Tuj1 marker (green) for the sample shown in (B). The inset shows a magnified view.

the density and the average length of neurites projecting from the cell body (Figure 2B). For DRG cultured in the absence and presence of Schwann cells, the average lengths of the neurites were  $208 \pm 24 \mu\text{m}$  and  $1879 \pm 281 \mu\text{m}$ , respectively (Figure S1, Supporting Information). High-magnification images of Schwann cells seeded on the scaffolds showed a consistent bipolar morphology and uniaxial alignment parallel to the nanofibers (Figure 2C). Double staining with S100 for Schwann cells and Tuj1 for neurites revealed that the neurites on the scaffold preseeded with Schwann cells were extended along both the Schwann cells and the underlying aligned fibers (Figure 2D). A direct interaction between the neurites and the oriented, preseeded Schwann cells was also confirmed by double staining of the neurites and the nuclei of Schwann cells (inset, Figure 2D).

**Outgrowth of DRG Neurites on Double-Layered Scaffolds in the Absence and Presence of Preseeded Schwann Cells.** We then fabricated and evaluated double-layered scaffolds consisting of aligned and random nanofibers in the top and bottom layers (denoted A/R) to imitate the unfolded structure of bilayer NGCs. For a more comprehensive understanding of the interaction between the neurites and nanofibers, we also fabricated double-layered scaffolds with uniaxially aligned nanofibers in both top and bottom layers with orthogonal orientations (denoted A/A). Extension of neurites was then examined for DRG cultured in the absence and presence of preseeded Schwann cells.

The inset in Figure 3A shows the SEM image of a typical A/R scaffold. Such a scaffold also supported neurite extension from DRG in both the absence and presence of preseeded Schwann cells (Figure 3, A and B). In the absence of Schwann cells, some short neurites were observed to project from the cell body, with most of the neurites extending parallel to the fibers in the top layer of the scaffold (Figure 3A). The neurites also showed a high degree of eccentricity and directional specificity, but their pattern of outgrowth was less ordered than that of

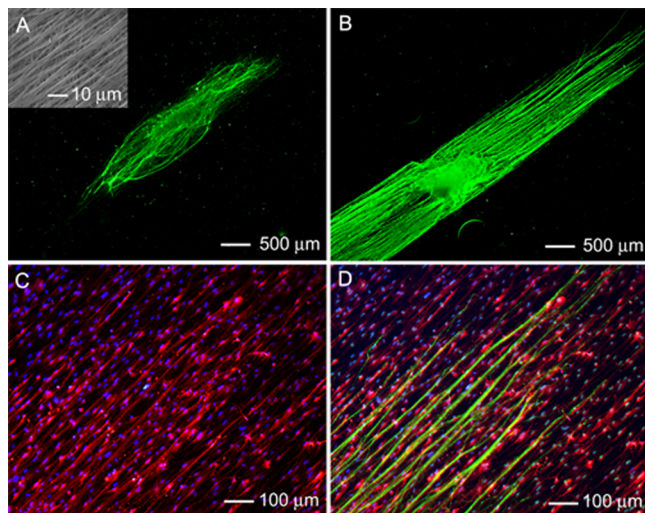


**Figure 3.** Fluorescence micrograph of the typical neurite field extending from DRG seeded on double-layered PCL nanofiber scaffolds (with aligned fibers in the top layer and random fibers in the bottom layer) in the (A) absence and (B) presence of preseeded Schwann cells. The neurites were stained with Tuj1 marker (green). Inset: SEM image of the nanofiber scaffold with aligned and random nanofibers in the top and bottom layers, respectively. (C) Double staining of the Schwann cells in (B) with anti-S100 (red) and their nuclei with DAPI (blue). (D) Triple staining of the Schwann cells with anti-S100 (red), their nuclei with DAPI (blue), and the neurites with Tuj1 marker (green) for the sample shown in (B).

neurites extending from the DRG cultured on the single-layered scaffold consisting only of uniaxially aligned nanofibers (Figure 2A). In comparison, the DRG cultured on an A/R scaffold preseeded with Schwann cells showed a significantly larger number of neurites extending from the cell body (Figure 3B). The average lengths of the neurites for the DRG cultured in the absence and presence of preseeded Schwann cells were  $144 \pm 46 \mu\text{m}$  and  $1843 \pm 137 \mu\text{m}$ , respectively (Figure S1, Supporting Information). The neurites extended parallel to the aligned nanofibers in the top layer of the scaffold, resulting in a highly eccentric neurite field. Staining with S100 demonstrated that the preseeded Schwann cells consistently assumed an elongated morphology and were aligned parallel to the individual nanofibers in the top layer of the scaffold (Figure 3C), similar to those in Figure 2C. Triple staining of Schwann cells, their nuclei, and the neurites revealed that the neurites were preferentially extended along both the elongated Schwann cells and aligned nanofibers in the top layer of the scaffold (Figure 3D). No evidence was found for neurites projecting in a direction other than parallel to the alignment of nanofibers.

We then examined neurite extension from DRG cultured on the double-layered A/A scaffolds, in which the nanofibers in different layers were oriented perpendicular to each other (inset in Figure 4A). The A/A scaffold also supported neurite extension from DRG in both the absence and presence of preseeded Schwann cells (Figure 4, A and B). Similar to the A/R scaffolds, the neurite fields projecting from DRG cultured on the A/A scaffolds exhibited a considerable degree of eccentricity and directional specificity, with neurites primarily extending along the alignment of the nanofibers in the top layer. In the presence of preseeded Schwann cells, a greater number of neurites were observed extending from the cell body, as compared to the previous group shown in Figure 4A. The average lengths of the neurites for the DRG cultured with

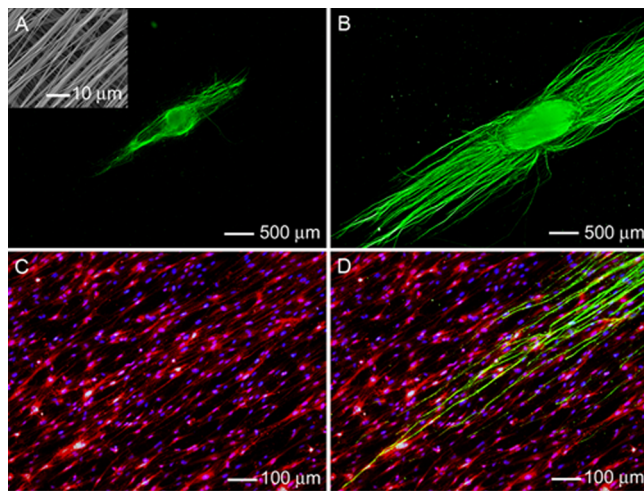


**Figure 4.** Fluorescence micrograph of the typical neurite field extending from DRG seeded on bilayer PCL nanofiber scaffolds with aligned fibers in both layers (oriented perpendicular to each other) in the (A) absence and (B) presence of preseeded Schwann cells. The neurites were stained with Tuj1 marker (green). Inset: SEM image of the double-layered nanofiber scaffold. (C) Double staining of the Schwann cells in (B) with anti-S100 (red) and their nuclei with DAPI (blue). (D) Triple staining of the Schwann cells with anti-S100 (red), their nuclei with DAPI (blue), and the neurites with Tuj1 marker (green) for the sample shown in (B).

and without the presence of Schwann cells were  $1934 \pm 167 \mu\text{m}$  and  $328 \pm 23 \mu\text{m}$ , respectively (Figure S1, Supporting Information). S100 staining of scaffolds preseeded with Schwann cells confirmed that the vast majority of cells assumed an elongated morphology and aligned parallel to individual nanofibers in the top layer of the scaffold rather than the bottom layer (Figure 4C). Triple staining further demonstrated that neurites projecting across the A/A scaffolds were extended primarily along the aligned nanofibers present in the top layer of the scaffold, similar to what was observed for the A/R scaffolds (Figure 4D). In the presence of preseeded Schwann cells, the neurites seem to interact very little with the nanofibers in the bottom layer of the A/A scaffolds. Otherwise, some neurites should have extended parallel to the alignment of nanofibers in the bottom layer, a direction perpendicular to that in the top layer.<sup>20</sup>

These results indicate that Schwann cells could not only enhance the outgrowth of neurites but also shield them from cues coming from the bottom layer of nanofibers. Recent studies have demonstrated the use of uniaxially aligned nanofibers to direct and enhance axonal outgrowth from cultured primary neurons *in vitro*,<sup>27–30</sup> however, NGCs constructed from a single layer of aligned nanofibers were prone to tearing during surgery. A more practical design should be based on the incorporation of a second layer of random nanofibers as a means to compensate for the poor surgical handling of uniaxially aligned nanofibers, although the inclusion of an additional layer of nanofibers with a different type of topography or orientation may have a negative impact on the neurite outgrowth.<sup>20</sup> Here we demonstrated that preseeding these double-layered scaffolds with Schwann cells could help mitigate the negative impact of the bottom layer of nanofibers (Figures 3B and 4B). Unlike neurites, Schwann cells preferentially conformed their morphology to the nanofibers in the topmost layer only (Figures 3C and 4C) regardless of the

topography or orientation for the nanofibers in the bottom layer. Once the inner surface of a bilayer NGC has been preseeded with Schwann cells, it should be able to effectively guide the extension of neurites during regeneration, similar to the conduit based on a single layer of aligned nanofibers.

**Morphologies of Schwann Cells Cultured on Different Types of Scaffolds.** To determine whether changes to the Schwann cell morphology as induced by the nanofiber-based scaffold were effectively translated into cytoskeletal remodeling, F-actin staining was applied. Double staining with rhodamine-phalloidin and 4',6-diamidino-2-phenylindole (DAPI) elucidated the cytoskeletal arrangement in Schwann cells seeded on the single-layered (random or aligned) and double-layered (A/R or A/A) scaffolds (Figure 5). The Schwann cells seeded on

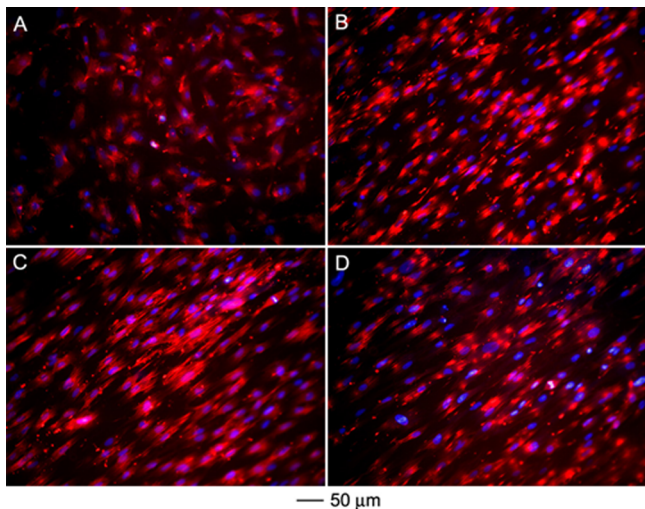


**Figure 5.** Cytoskeletal arrangement of the Schwann cells preseeded on (A) random nanofibers, (B) aligned nanofibers, (C) double-layered nanofiber scaffolds with aligned and random fibers in the top and bottom layers, respectively, and (D) double-layered nanofiber scaffolds with aligned fibers in both layers but oriented perpendicular to each other. The actin cytoskeleton and nuclei of the Schwann cells were stained with rhodamine phalloidin (red) and DAPI (blue), respectively.

scaffolds of random nanofibers demonstrated a disorganized actin meshwork, in agreement with the observations of random organization and minimal alignment (Figure 5A and Figure 1C). In contrast, the Schwann cells seeded on the aligned nanofibers showed an aligned actin network consisting of a large number of filaments aligned parallel to the long axis of the underlying nanofibers (Figure 5B). The observation of cytoskeletal alignment parallel to individual nanofibers in the scaffolds largely agrees with our observations of cell elongation and alignment by S100 staining, suggesting that the Schwann cells had indeed responded to the topographical cue presented by the aligned nanofibers. Interestingly, the actin cytoskeletons of Schwann cells seeded on both A/R and A/A double-layered scaffolds essentially mirrored that of cells seeded on a single-layered scaffold consisting of aligned nanofibers (Figure 5, C and D). In both cases, the Schwann cells exhibited multiple actin filaments oriented parallel to the long axis of nanofibers in the top layer of the scaffolds, confirming the predominant interactions between the seeded cells with the top layer of the scaffolds.

Schwann cells can secrete neurotrophic factors, remodel and deposit ECM proteins, and interact with macrophages to remove debris during Wallerian degeneration, facilitating neuroregeneration.<sup>31–36</sup> Several studies have shown that silicone microgrooves, ECM microstripes (e.g., laminin), and polymer fibers with diameters on the microscale can spatially organize Schwann cells through contact guidance.<sup>31,35–41</sup> More recently, aligned electrospun nanofibers were found to enhance Schwann cell migration and maturation *in vitro* through the presentation of topographical cues,<sup>31,42,43</sup> however, these studies did not look at the effect of scaffolds containing more than one layer of nanofibers on the morphology and cytoskeleton arrangement of the Schwann cells, disregarding the neuroregenerative potential of NGCs constructed from double-layered scaffolds. The present study demonstrated that double-layered scaffolds containing aligned nanofibers in the top layer could spatially align the cytoskeleton of the Schwann cells preseeded on the scaffolds, regardless of the topography of nanofibers in the bottom layer.

**Nerve Repair Using Bilayer NGCs in the Absence and Presence of Preseeded Schwann Cells in a Sciatic Nerve Injury/Repair Model.** Bilayer NGCs were fabricated from the A/R scaffolds and tested *in vivo*. A schematic of such NGCs can be found in Figure 6A. The efficiency of the bilayer NGCs in facilitating nerve regeneration was evaluated through the microsurgical repair of a critical nerve gap of 14 mm. Three experimental groups were examined, including isografts and bilayer NGCs with and without preseeded Schwann cells. Assessment of regenerative nerve tissue at distal stump 12 weeks post-operatively further provided a useful measure of the ability of the NGCs to support chronic nerve regeneration in a clinically relevant setting.

Histomorphometric examination of the regenerative nerve tissue 5 mm distal to the implanted nerve graft or NGCs provided a comprehensive assessment of the quality of successful axonal regeneration across the critical nerve defects. Representative histological sections demonstrated a significant disparity in both the number and quality of the regenerated nerve fibers in the three groups (Figure 6, B–D). Nerve tissue distal to the implanted fresh nerve isograft demonstrated the highest number of regenerative nerve fibers. Nerve fibers extending through the implanted fresh nerve isograft were also noted to be larger in diameter and occupy a greater percentage of the total nerve tissue. For the two groups of repair with the bilayer NGCs, nerve tissues distal to the implanted NGCs also demonstrated a considerable level of regeneration. Regenerative nerve fibers observed distal to the NGCs with preseeded Schwann cells were noted to be equivalent in diameter and maturity to those observed distal to the NGCs without preseeded Schwann cells. It is worth mentioning that the number of regenerated nerve fibers distal to the NGCs seeded with Schwann cells was fewer than those distal to the fresh nerve isograft and additionally had a lower average diameter.

Quantitative analysis of the number of nerve fibers present midgraft/midconduit and 5 mm distal to the implanted graft/conduits confirmed these results (Figure 6E). The fresh nerve isograft was observed to support  $17\ 168 \pm 268$  and  $8663 \pm 998$  myelinated nerve fibers midgraft and 5 mm distal to the graft, respectively. In contrast, bilayer NGCs without preseeded Schwann cells supported  $4817 \pm 3725$  and  $1864 \pm 1250$  myelinated fibers, while the Schwann cell-seeded NGCs supported  $9277 \pm 2833$  and  $3472 \pm 2082$  myelinated fibers midconduit and 5 mm distal to the conduit, respectively. These

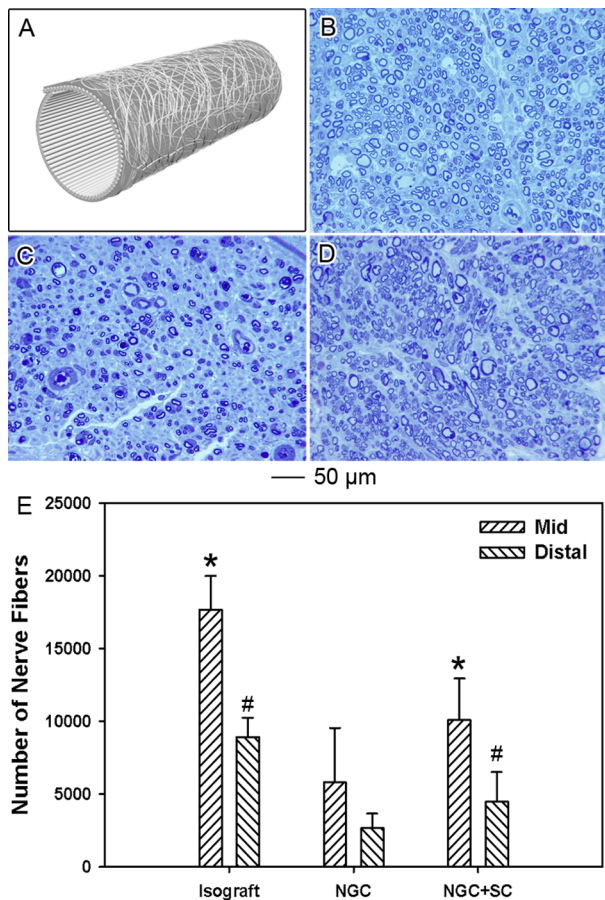


**Figure 6.** Histomorphometric analysis of the regenerated peripheral nerve tissue 12 weeks post-operation. (A) Schematic of the bilayer NGCs used in the present work. (B–D) Representative histological sections of the regenerated peripheral nerve tissue harvested 5 mm distal to interposed (B) fresh nerve isograft, (C) bilayer NGC, and (D) bilayer NGC preseeded with Schwann cells (NGC+SC). (E) Nerve fiber counts performed on histological sections collected in the middle point of graft or conduit and 5 mm distal to implanted graft/conduits. \* indicates  $p < 0.05$  for samples preseeded with Schwann cells compared with samples without Schwann cells under the same condition; # indicates  $p < 0.05$  for samples compared with bilayer NGC at 5 mm distal to the graft/conduit.

results indicated that while the isograft group outperformed both NGC groups the presence of Schwann cells inside bilayer NGCs could greatly promote the sprouting of the regenerating nerve fibers.

We further measured the evoked muscle force in the denervated/reinnervated musculature within the sciatic nerve distribution to assess the degree to which the various nerve graft/conduits promoted functional regeneration of peripheral motor axons across critical nerve defects (Figure 7A). Additionally, evoked muscle force provides a viable metric for effective post-operative motor recovery, an important outcome in assessing clinical viability of various nerve repair techniques. Twelve weeks post-operatively, extensor digitorum longus (EDL) muscles innervated by sciatic nerves repaired with fresh nerve isografts demonstrated a maximum isometric tetanic force production of  $1.37 \pm 0.14$  N, approximately  $36.3 \pm 3.7\%$  of maximal force production evoked by healthy controls. EDL muscles innervated by sciatic nerves repaired with bilayer NGCs without preseeded Schwann cells demonstrated maximum isometric tetanic force production of  $0.59 \pm 0.29$

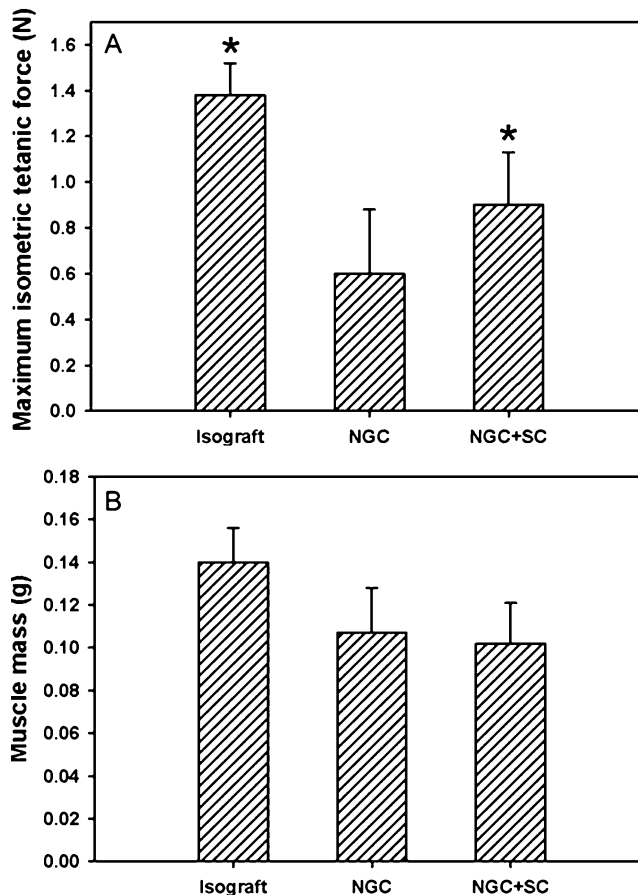


**Figure 7.** Functional motor recovery in denervated or reinnervated extensor digitorum longus (EDL) muscle 12 weeks post-operation. (A) Maximum isometric tetanic force production in the EDL muscle following electrical stimulation of the repaired sciatic nerve. (B) Assessment of muscle mass in the EDL muscle following denervation or reinnervation. \* indicates  $p < 0.05$  for groups compared with the NGC group.

N, approximately  $15.6 \pm 7.7\%$  of healthy controls. Implantation of bilayer NGCs preseeded with Schwann cells was demonstrated to enable maximum isometric tetanic force production of  $0.88 \pm 0.26$  N in reinnervated EDL muscle, approximately  $23.3 \pm 6.9\%$  of healthy controls.

Measurements of muscle mass were also performed, following functional assessment, to characterize the degree of muscle atrophy experienced following peripheral nerve repair utilizing various nerve grafts/conduits (Figure 7B). EDL muscles innervated by sciatic nerves repaired with fresh nerve isograft experienced the lowest amount of net muscle atrophy  $0.139 \pm 0.014$  g, retaining  $67.3 \pm 6.8\%$  of healthy muscle mass. Both NGC groups encouraged similar degrees of muscle preservation. While the NGC group without pre-seeded Schwann cells supported EDL muscle masses of  $0.105 \pm 0.023$  g,  $50.8 \pm 11.1\%$  of control, the NGCs pre-seeded with Schwann cells supported EDL muscle masses of  $0.104 \pm 0.022$  g,  $50.4 \pm 10.7\%$  of control.

Prior in vivo investigations commonly utilized NGCs composed only of aligned nanofibers to repair peripheral nerve defects in rats.<sup>44,45</sup> In the present study, we demonstrated that bilayer NGCs with random nanofibers in the outer layer and aligned nanofibers in the inner wall not only resisted the tearing forces during surgery but also successfully bridged a 14

mm lesion in a primary rat sciatic nerve injury/repair model and mediated moderate functional recovery. Furthermore, the present work also indicated the efficacy of the bilayer NGCs in re-establishing functional connections to distal musculature and restoring normal physiological musculoskeletal function. Measurements of evoked muscle force production provide a comprehensive and reliable means of assessing nerve regeneration, functional reinnervation, and muscle preservation post-operatively. When combined with Schwann cell therapy, bilayer NGCs promoted improved force production in distal musculature following nerve transection/repair. These results conclusively demonstrated the ability of the bilayer NGCs to encourage robust functional recovery post-operatively. Given that motor recovery is the most desirable outcome following peripheral nerve repair in humans, the present work provided significant evidence that the presence of Schwann cells improved the clinical efficacy of bilayer NGCs and that Schwann cell seeded bilayer NGCs possess significant potential as future methods for peripheral nerve repair.

## CONCLUSIONS

Bilayer NGCs with random nanofibers in the outer layer and uniaxially aligned nanofibers in the inner layer were more tear-resistant during surgical procedures as compared with the NGCs composed of solely uniaxially aligned nanofibers. However, the random nanofibers could interfere with the aligned nanofibers to influence the patterns of neurite outgrowth and impede axonal regeneration. The influence of the random nanofibers could be diminished by preseeding the inner surface of a bilayer NGC with Schwann cells because both the morphology and cytoskeleton structure of Schwann cells were only affected by the topmost layer of fibers. As long as the Schwann cells were in direct contact with the aligned nanofibers, they could direct the neurites to extend in the direction parallel to the alignment of nanofibers in the topmost layer. These findings were reflected in the results from *in vivo* assessments of the bilayer NGCs. Once seeded with autologous Schwann cells, the bilayer NGCs could effectively improve both nerve fiber sprouting and motor recovery following implantation in a sciatic nerve injury/repair model. Altogether, the current study suggests that bilayer NGCs preseeded with Schwann cells can serve as a practical and clinically viable tool for enhancing regenerative outcomes in peripheral nerve repair.

## ASSOCIATED CONTENT

### Supporting Information

Average lengths of DRG neurites cultured on various nanofiber scaffolds with and without the presence of preseeded Schwann cells. This material is available free of charge via the Internet at <http://pubs.acs.org>.

## AUTHOR INFORMATION

### Corresponding Author

\*E-mail: younan.xia@bme.gatech.edu.

### Present Address

<sup>#</sup>Mary and Dick Holland Regenerative Medicine Program and Department of Pharmaceutical Sciences, University of Nebraska Medical Center, Omaha, Nebraska 68198, United States.

### Author Contributions

<sup>†</sup>Authors J. Xie and M. R. MacEwan contributed equally to this work.

## Author Contributions

J.X. fabricated the scaffolds/conduits, conducted the *in vitro* study, and prepared the first draft of the manuscript; M.R.M. isolated the DRG, performed the *in vivo* study, and revised the manuscript; W.L. fabricated some of the scaffolds/conduits, was involved in the *in vitro* study, and revised the manuscript; N.J. was involved in some of the staining experiments; X.L. fabricated some of the scaffolds/conduits and was involved in the *in vitro* study; D.H. was involved in the *in vivo* study; and Y.X. supervised the entire project, was involved in the design of all experiments, and finalized the manuscript.

## Notes

The authors declare no competing financial interest.

## ACKNOWLEDGMENTS

This work was supported by a 2006 NIH Director's Pioneer Award (DP1 OD000798) and start-up funds from Washington University in St. Louis. We thank Dr. Shelly Sakiyama-Elbert for her help during the preparation of this manuscript.

## REFERENCES

- (1) Burnett, M. G.; Zager, E. L. Pathophysiology of Peripheral Nerve Injury: A Brief Review. *Neurosurg. Focus* **2004**, *16*, 1–7.
- (2) Noble, J.; Munro, C. A.; Prasad, V. S.; Midha, R. Analysis of Upper and Lower Extremity Peripheral Nerve Injuries in a Population of Patients with Multiple Injuries. *J. Trauma Acute Care Surg.* **1998**, *45*, 116–122.
- (3) Schmidt, C. E.; Leach, J. B. Neural Tissue Engineering: Strategies for Repair and Regeneration. *Annu. Rev. Biomed. Eng.* **2003**, *5*, 293–347.
- (4) Daly, W.; Yao, L.; Zeugolis, D.; Windebank, A.; Pandit, A. A Biomaterials Approach to Peripheral Nerve Regeneration: Bridging the Peripheral Nerve Gap and Enhancing Functional Recovery. *J. R. Soc., Interface* **2012**, *9*, 202–221.
- (5) Evans, G. R. D. Challenges to Nerve Regeneration. *Semin. Surg. Oncol.* **2000**, *19*, 312–318.
- (6) Hadlock, T.; Elisseeff, J.; Langer, R.; Vacanti, J.; Cheney, M. A. Tissue–Engineered Conduit for Peripheral Nerve Repair. *Arch. Otolaryngol., Head Neck Surg.* **1998**, *124*, 1081–1086.
- (7) Bellamkonda, R. V. Peripheral Nerve Regeneration: An Opinion on Channels, Scaffolds and Anisotropy. *Biomaterials* **2006**, *27*, 3515–3518.
- (8) Mackinnon, S. E.; Dellon, A. L. Clinical Nerve Reconstruction with a Bioabsorbable Polyglycolic Acid Tube. *Plast. Reconstr. Surg.* **1990**, *85*, 419–424.
- (9) Liu, W.; Thomopoulos, S.; Xia, Y. Electrospun Nanofibers for Regenerative Medicine. *Adv. Healthcare Mater.* **2012**, *1*, 10–25.
- (10) Rodríguez, F. J.; Verdú, E.; Ceballos, D.; Navarro, X. Nerve Guides Seeded with Autologous Schwann Cells Improve Nerve Regeneration. *Exp. Neurol.* **2000**, *161*, 571–584.
- (11) Xie, J.; MacEwan, M. R.; Schwartz, A. G.; Xia, Y. Electrospun Nanofibers for Neural Tissue Engineering. *Nanoscale* **2010**, *2*, 35–44.
- (12) Yang, F.; Murugan, R.; Wang, S.; Ramakrishna, S. Electrospinning of Nano/Micro Scale Poly(L-lactic acid) Aligned Fibers and Their Potential in Neural Tissue Engineering. *Biomaterials* **2005**, *26*, 2603–2610.
- (13) Pham, Q. P.; Sharma, U.; Mikos, A. G. Electrospinning of Polymeric Nanofibers for Tissue Engineering Applications: A Review. *Tissue Eng.* **2006**, *12*, 1197–1211.
- (14) Li, D.; Xia, Y. Electrospinning of Nanofibers: Reinventing the Wheel? *Adv. Mater.* **2004**, *16*, 1151–1170.
- (15) Li, D.; McCann, J. T.; Xia, Y.; Marquez, M. Electrospinning: A Simple and Versatile Technique for Producing Ceramic Nanofibers and Nanotubes. *J. Am. Ceram. Soc.* **2006**, *89*, 1861–1869.
- (16) Li, D.; Wang, Y.; Xia, Y. Electrospinning of Polymeric and Ceramic Nanofibers as Uniaxially Aligned Arrays. *Nano Lett.* **2003**, *3*, 1167–1171.

- (17) Li, D.; Ouyang, G.; McCann, J. T.; Xia, Y. Collecting Electrospun Nanofibers with Patterned Electrodes. *Nano Lett.* **2005**, *5*, 913–916.
- (18) Dai, Y.; Liu, W.; Formo, E.; Sun, Y.; Xia, Y. Ceramic Nanofibers Fabricated by Electrospinning and Their Applications in Catalysis, Environmental Science, and Energy Technology. *Polym. Adv. Technol.* **2011**, *22*, 326–338.
- (19) Li, D.; Wang, Y.; Xia, Y. Electrospinning Nanofibers as Uniaxially Aligned Arrays and Layer-by-Layer Stacked Films. *Adv. Mater.* **2004**, *16*, 361–366.
- (20) Xie, J.; MacEwan, M. R.; Li, X.; Sakiyama-Elbert, S. E.; Xia, Y. Neurite Outgrowth on Nanofiber Scaffolds with Different Orders, Structures, and Surface Properties. *ACS Nano* **2009**, *3*, 1151–1159.
- (21) Xie, J.; MacEwan, M. R.; Willerth, S. M.; Li, X.; Moran, D. W.; Sakiyama-Elbert, S. E.; Xia, Y. Conductive Core–Sheath Nanofibers and Their Potential Application in Neural Tissue Engineering. *Adv. Funct. Mater.* **2009**, *19*, 2312–2318.
- (22) Xie, J.; Willerth, S. M.; Li, X.; MacEwan, M. R.; Rader, A.; Sakiyama-Elbert, S. E.; Xia, Y. The Differentiation of Embryonic Stem Cells Seeded on Electrospun Nanofibers into Neural Lineages. *Biomaterials* **2009**, *30*, 354–362.
- (23) Hunter, D. A.; Moradzadeh, A.; Whitlock, E. L.; Brenner, M. J.; Myckatyn, T. M.; Wei, C. H.; Tung, T. H.; Mackinnon, S. E. Binary Imaging Analysis for Comprehensive Quantitative Histomorphometry of Peripheral Nerve. *J. Neurosci. Methods* **2007**, *166*, 116–124.
- (24) Donato, R. Intracellular and Extracellular Roles of S100 Proteins. *Microsc. Res. Technol.* **2003**, *60*, 540–551.
- (25) Bhattacharyya, A.; Oppenheim, R. W.; Prevette, D.; Moore, B. W.; Brackenbury, R.; Ratner, N. S100 is Present in Developing Chicken Neurons and Schwann Cell and Promotes Motor Neuron Survival *in vivo*. *J. Neurobiol.* **1992**, *23*, 451–466.
- (26) Armin, A.; Connelly, E. M.; Rowden, G. An Immunoperoxidase Investigation of S-100 Protein in Granular Cell Myoblastomas: Evidence for Schwann Cell Derivation. *Am. J. Clin. Pathol.* **1983**, *1*, 37–44.
- (27) Corey, J. M.; Lin, D. Y.; Mycek, K. B.; Chen, Q.; Samuel, S.; Feldman, E. L.; Martin, D. C. Aligned Electrospun Nanofibers Specify the Direction of Dorsal Root Ganglia Neurite Growth. *J. Biomed. Mater. Res., Part A* **2007**, *83*, 636–645.
- (28) Jha, B. S.; Colello, R. J.; Bowman, J. R.; Sell, S. A.; Lee, K. D.; Bigbee, J. W.; Bowlin, G. L.; Chow, W. N.; Mather, B. E.; Simpson, D. G. Two Pole Air Gap Electrospinning: Fabrication of Highly Aligned, Three-Dimensional Scaffolds for Nerve Reconstruction. *Acta Biomater.* **2011**, *7*, 203–215.
- (29) Wang, H. B.; Mullins, M. E.; Cregg, J. M.; Hurtado, A.; Oudega, M.; Trombley, M. T.; Gilbert, R. J. Creation of Highly Aligned Electrospun Poly-L-lactic Acid Fibers for Nerve Regeneration Applications. *J. Neural Eng.* **2009**, *6*, 016001.
- (30) Patel, S.; Kurpinski, K.; Quigley, R.; Gao, H.; Hsiao, B. S.; Poo, M. M.; Li, S. Bioactive Nanofibers: Synergistic Effects of Nanotopography and Chemical Signaling on Cell Guidance. *Nano Lett.* **2007**, *7*, 2122–2128.
- (31) Thompson, D. M.; Buettner, H. M. Neurite Outgrowth is Directed by Schwann Cell Alignment in the Absence of Other Guidance Cues. *Annu. Biomed. Eng.* **2006**, *34*, 161–168.
- (32) Chernousov, M. A.; Rothblum, K.; Tyler, W. A.; Stahl, R. C.; Carey, D. J. Schwann Cells Synthesize Type V Collagen That Contains a Novel Alpha4 Chain: Molecular Cloning, Biochemical Characterization and High Affinity Heparin Binding of Alpha4 (V) Collagen. *J. Biol. Chem.* **2000**, *275*, 28208–28215.
- (33) Stoll, G.; Müller, H. W. Nerve Injury, Axonal Degeneration and Neural Regeneration: Basic Insights. *Brain Pathol.* **1999**, *9*, 313–325.
- (34) Chamberlain, L.; Yannas, I.; Hsu, H.; Strichartz, G.; Spector, M. Collagen–GAG Substrate Enhances the Quality of Nerve Regeneration Through Collagen Tubes up to Level of Autograft. *Exp. Neurol.* **1998**, *154*, 315–329.
- (35) Miller, C.; Jeftinija, S.; Mallapragada, S. Micropatterned Schwann Cell–Seeded Biodegradable Polymer Substrates Significantly Enhance Neurite Alignment and Outgrowth. *Tissue Eng.* **2001**, *7*, 705–715.
- (36) Schmalenberg, K. E.; Uhrich, K. E. Micropatterned Polymer Substrates Control Alignment of Proliferating Schwann Cells to Direct Neuronal Regeneration. *Biomaterials* **2005**, *26*, 1423–1430.
- (37) Ni, H. C.; Lin, Z. Y.; Hsu, S. H.; Chiu, I. M. The Use of Air Plasma in Surface Modification of Peripheral Nerve Conduits. *Acta Biomater.* **2010**, *6*, 2066–2076.
- (38) Miller, C.; Shanks, H.; Witt, A.; Rutkowski, G.; Mallapragada, S. Oriented Schwann Cell Growth on Micropatterned Biodegradable Polymer Substrates. *Biomaterials* **2001**, *22*, 1263–1269.
- (39) Gupta, D.; Venugopal, J.; Prabhakaran, M. P.; Dev, V.; Low, S.; Choon, A. T.; Ramakrishna, S. Aligned and Random Nanofibrous Substrate for the *in vitro* Culture of Schwann Cells for Neural Tissue Engineering. *Acta Biomater.* **2009**, *5*, 2560–2569.
- (40) Bozkurt, A.; Deumens, R.; Beckmann, C.; Olde Damink, L.; Schügner, F.; Heschel, I.; Sellhaus, B.; Weis, J.; Jahnen-Decent, W.; Brook, G. A. *In vitro* Cell Alignment Obtained with a Schwann Cell Enriched Microstructured Nerve Guide with Longitudinal Guidance Channels. *Biomaterials* **2009**, *30*, 169–179.
- (41) Ahmed, Z.; Brown, R. A. Adhesion, Alignment, and Migration of Cultured Schwann Cells on Ultrathin Fibronectin Fibres. *Cell Motil. Cytoskeleton* **1999**, *42*, 331–343.
- (42) Bruder, J. M.; Lee, A. P.; Hoffman-Kim, D. Biomimetic Materials Replicating Schwann Cell Topography Enhance Neuronal Adhesion and Neurite Alignment *in vitro*. *J. Biomater. Sci., Polym. Ed.* **2007**, *18*, 967–982.
- (43) Chew, S. Y.; Mi, R.; Hoke, A.; Leong, K. W. The Effect of the Alignment of Electrospun Fibrous Scaffolds on Schwann Cell Maturation. *Biomaterials* **2008**, *29*, 653–661.
- (44) Yu, X.; Bellamkonda, R. V. Tissue–Engineered Scaffolds are Effective Alternatives to Autografts for Bridging Peripheral Nerve Gaps. *Tissue Eng.* **2003**, *9*, 421–430.
- (45) Hoffman-Kim, D.; Mitchel, J. A.; Bellamkonda, R. V. Topography, Cell Response, and Nerve Regeneration. *Annu. Rev. Biomed. Eng.* **2010**, *12*, 203–231.